REPORT

SOLID-STATE PHYSICS

A parity-breaking electronic nematic phase transition in the spin-orbit coupled metal Cd$_2$Re$_2$O$_7$

J. W. Harter,[1,2] Z. Y. Zhao,[3,4] J.-Q. Yan,[3,5] D. G. Mandrus,[3,5] D. Hsieh[1,2]*

Strong electron interactions can drive metallic systems toward a variety of well-known symmetry-broken phases, but the instabilities of correlated metals with strong spin-orbit coupling have only recently begun to be explored. We uncovered a multipolar nematic phase of matter in the metallic pyrochlore Cd$_2$Re$_2$O$_7$ using spatially resolved second-harmonic optical anisotropy measurements. Like previously discovered electronic nematic phases, this multipolar phase spontaneously breaks rotational symmetry while preserving translational invariance. However, it has the distinguishing property of being odd under spatial inversion, which is allowed only in the presence of spin-orbit coupling. By examining the critical behavior of the multipolar nematic order parameter, we show that it drives the thermal phase transition near 200 kelvin in Cd$_2$Re$_2$O$_7$ and induces a parity-breaking lattice distortion as a secondary order.

In the presence of strong Coulomb interactions, the fluid of mobile electrons in a metal can spontaneously break the point group symmetries of the underlying crystal lattice, realizing the quantum analog of a nematic liquid crystal (1). Like their classical counterparts, quantum nematic phases generally preserve spatial inversion symmetry and are therefore anisotropic but centrosymmetric fluids. Experimental evidence of such nematic order was first detected in a two-dimensional (2D) GaAs/AlGaAs quantum well interface on the basis of a pronounced resistivity anisotropy between the two principal directions of the underlying square lattice (2, 3). Subsequently, similar behavior has been reported in a number of quasi-2D square lattice compounds, including Sr$_3$Ru$_2$O$_7$ (4), URu$_2$Si$_2$ (5), and several families of both copper- (6, 7) and iron-based (8–11) high-temperature superconductors, suggesting possible connections between even-parity nematic fluctuations and unconventional s- and d-wave Cooper pairing (12).

Extending earlier work on Fermi liquid instabilities in the p-wave spin interaction channel (13), it has recently been predicted that correlated metals with strong spin-orbit coupling may realize a fundamentally new class of electronic nematic phases with spontaneously broken spatial inversion symmetry (14), including a quantum analog of the unusual N$_T$ nematic phase discussed in the context of classical bent-core liquid crystals (15). Theoretical models have shown that parity-breaking nematic fluctuations can induce odd-parity p- or f-wave Cooper pairing and thus provide a route to topological superconductivity (16, 17). In addition, because inversion symmetry-breaking necessarily lifts the spin degeneracy of bulk energy bands in a spin-orbit coupled system, odd-parity nematic order offers a potential mechanism for generating topologically protected Weyl and nodal-line semimetals and for designing highly tunable charge-to-spin current conversion technologies for spintronics applications.

The order parameter for this predicted new class of spin-orbit–coupled parity-breaking electronic nematic phases—so-called "multipolar" nematics (14)—can be represented by a symmetric traceless second-rank pseudotensor Q_{ij} that is odd under spatial inversion. This order parameter induces a deformation and spin splitting of the Fermi surface via the spin-orbit interaction Hamiltonian $H_{SO} = \sum_{ij} Q_{ij}\sigma_i k_j$, where σ_i are the Pauli matrices and k_j is the crystal momentum (14, 18). In a cubic material, for example, this order parameter can have either E_u or T_{2u} symmetry. An example of a spin-polarized Fermi surface distortion induced by T_{2u} multipolar nematic order is shown in Fig. 1A.

The correlated metallic pyrochlore Cd$_2$Re$_2$O$_7$ has been proposed as a candidate for hosting multipolar nematic order because of the strong spin-orbit coupling of Re 5d valence electrons. Detailed Raman scattering (19), x-ray (20, 21) and neutron (22) diffraction, and optical second-harmonic generation (SHG) (23) studies have shown that at critical temperature (T_c) ~ 200 K, the material undergoes a continuous phase transition from a centrosymmetric cubic structure (space group $Fd\bar{3}m$) to a noncentrosymmetric tetragonal structure (space group $I\bar{4}m2$) that breaks threefold rotational symmetry about the 111 axis (Fig. 1, B and C). This phase transition has traditionally been attributed to the freezing of a soft phonon mode with E_u symmetry, dominated by the displacement of O(1) atoms (19, 24, 25). However, the observation of extremely small changes in lattice parameters (21, 22), an anomalous temperature dependence of superlattice Bragg peaks (20), and a dramatic reduction in the electronic density of states across T_c (26–29) calls this interpretation into question and raises the possibility that a hitherto undetected electronic order is driving the transition.
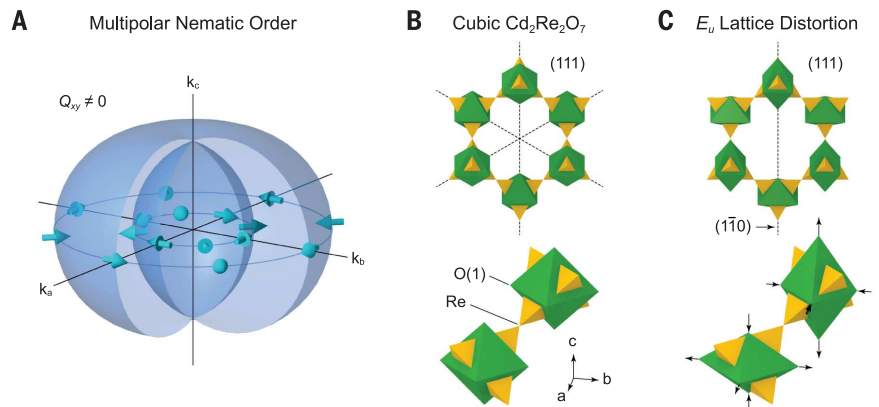

Fig. 1. Illustration of electronic and structural order parameters in Cd$_2$Re$_2$O$_7$. (**A**) T_{2u} distortion of a spherical Fermi surface induced by a Q_{xy} multipolar nematic order parameter. The Fermi surface is split into two nondegenerate surfaces of opposite spin texture (arrows), with the largest splitting at the equator and zero splitting at the poles. (**B**) The ideal pyrochlore structure of Cd$_2$Re$_2$O$_7$ viewed along the (111) axis. Only Re (yellow tetrahedra) and O(1) (green octahedra) sublattices are shown. Dashed lines depict mirror planes. For clarity, an enlarged view of two neighboring subunits from an alternative angle is also displayed. (**C**) The effect of the E_u lattice distortion. The vertical dashed line depicts the preserved ($1\bar{1}0$) mirror plane, and arrows show the displacement directions of the O(1) atoms.

[1]Department of Physics, California Institute of Technology, Pasadena, CA 91125, USA. [2]Institute for Quantum Information and Matter, California Institute of Technology, Pasadena, CA 91125, USA. [3]Materials Science and Technology Division, Oak Ridge National Laboratory, Oak Ridge, TN 37831, USA. [4]Department of Physics and Astronomy, University of Tennessee, Knoxville, TN 37996, USA. [5]Department of Materials Science and Engineering, University of Tennessee, Knoxville, TN 37996, USA.
*Corresponding author. Email: dhsieh@caltech.edu

Unlike the previously studied even-parity nematic phases, multipolar nematic order cannot be experimentally identified by using charge transport anisotropy measurements because the loss of inversion symmetry is manifested in the spin texture of the Fermi surface. Moreover, observations of conventional nematic order have often relied on an alignment of nematic directors by using applied magnetic (4) or uniaxial strain (9) fields in order to measure macroscopic symmetry-breaking responses, but neither magnetic nor strain fields couple linearly to Q_{ij} because they are parity-even. Nonlinear optical anisotropy measurements can overcome these challenges because they probe the structure of higher-rank susceptibility tensors that contain full point group information (30) and can be performed in a spatially resolved manner. Optical SHG is particularly well-suited to identifying odd-parity phases because the leading-order electric dipole contribution, which is described by a third-rank susceptibility tensor relating the incident electric field to the nonlinear polarization induced at twice the incident frequency via the equation $P_i(2\omega) = \chi_{ijk}E_j(\omega)E_k(\omega)$, is only allowed if inversion symmetry is broken. Because of this property, optical SHG has been used recently to study noncentrosymmetric Weyl semimetals (31) and odd-parity order in correlated iridates and cuprates (32, 33). To completely resolve the structure of χ_{ijk} for $Cd_2Re_2O_7$, we used a recently developed high-speed rotational anisotropy (RA) technique (34, 35) that involves focusing a beam of light obliquely onto the surface of a single crystal and measuring variations in the intensity of reflected SHG light as the scattering plane is rotated about the surface normal. By projecting the SHG signal radiated at different scattering plane angles ϕ onto a circular locus of points on a stationary 2D detector (Fig. 2A), the experiment can be carried out at very high rotational frequencies (~4 Hz), which greatly enhances the sensitivity to small changes in symmetry by averaging over laser fluctuations.

In order to isolate a single-phase domain for detailed RA-SHG study, we carried out three successive stages of microscopy on the natural (111) facet of a $Cd_2Re_2O_7$ single crystal grown by means of vapor transport [section S1 of (36)]. First, white-light microscopy was used to select a smooth area free of surface striations (Fig. 2B). Next, wide-field SHG images [section S2 of (36)] were acquired on this area both above and below T_c (Fig. 2C). For $T > T_c$, the SHG signal is dominated by the electric dipole response at the surface (χ_{ijk}^S), where inversion symmetry is necessarily broken. The observed spatial uniformity of the intensity indicates a single cubic structural domain. For $T < T_c$, a strong bulk response (χ_{ijk}^B) develops owing to the inversion-symmetry–breaking tetragonal distortion. Three types of tetragonal domains with sharply defined linear boundaries are clearly resolved, associated with orientations of the main tetragonal axis along each of the three equivalent cubic lattice directions [section S4 of (36)]. Last, we performed scanning RA-SHG measurements [section S3 of (36)] within a single tetragonal domain. Because inversion symmetry is spontaneously broken at the phase transition, domains with opposite parity, which we label (+) or (−), will naturally form. Because the sign of χ_{ijk}^B reverses upon spatial inversion, these parity domains exhibit distinct SHG responses ($\chi_{ijk} = \chi_{ijk}^S \pm \chi_{ijk}^B$) arising from interference between the surface and bulk terms.
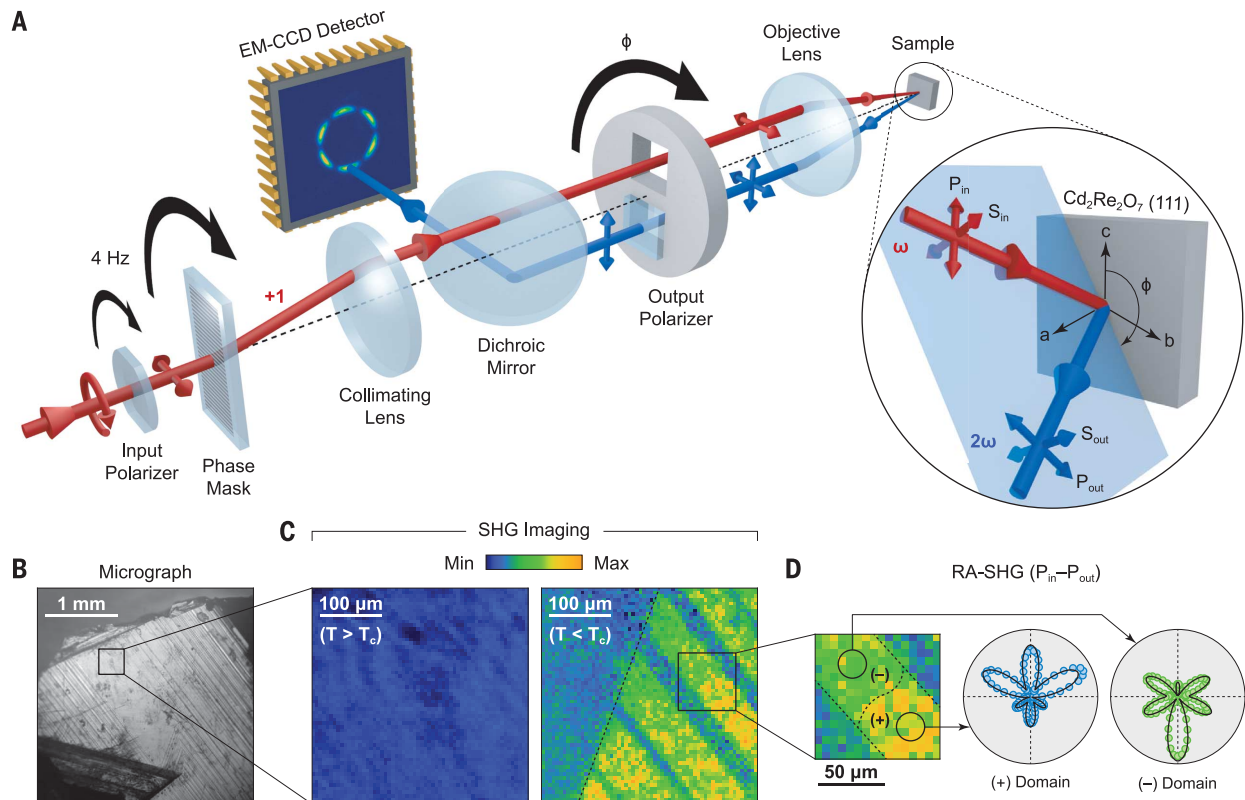
Fig. 2. Spatially resolved optical SHG anisotropy measurements. (**A**) Schematic of the RA-SHG setup. A circularly polarized laser beam (red) with center wavelength at 800 nm is sent through a linear polarizer (to select either P_{in} or S_{in} polarization) and onto a phase mask. The +1 diffracted order is isolated and redirected parallel to the optical axis by a collimating lens. After passing through a dichroic mirror, the beam is focused by an objective lens onto the stationary sample to a spot size of ~30 μm. The reflected SHG beam (blue) is recollimated by the objective, passes through a second linear polarizer (to select either P_{out} or S_{out} polarization), and is deflected by the dichroic mirror onto a 2D electron-multiplying charge-coupled device (EMCCD) camera. The polarizers and phase mask rotate rapidly (black arrows), causing the SHG beam to trace out a circle on the camera as the scattering plane angle ϕ changes. (**B**) Optical micrograph of the (111) surface of a $Cd_2Re_2O_7$ single crystal. (**C**) Wide-field SHG image of a striation-free region measured at $T = 210$ K and $T = 150$ K. All three types of tetragonal domains [section S4 of (36)] are visible in the low-temperature image. (**D**) Enlarged SHG image of the region over which scanning RA-SHG was performed. P_{in}–P_{out} RA-SHG patterns for two opposite parity domains are shown, and an approximate domain boundary is drawn.

This in turn produces distinct RA-SHG patterns (Fig. 2D).

To finely resolve the symmetries broken across T_c, we performed detailed temperature-dependent RA-SHG measurements on a single domain using different combinations of incoming (in) and outgoing (out) light polarizations, which can be either parallel (P) or perpendicular (S) to the scattering plane [Fig. 2A and section S5 of (36)]. Examples of RA-SHG patterns acquired with a S_{in}–P_{out} polarization geometry for a selection of temperatures near T_c are shown in Fig. 3. For $T > T_c$, the raw RA-SHG images show disconnected arcs centered at $\phi = 0°$ and every 60° interval (Fig. 3A). A polar plot of SHG intensity versus ϕ extracted from the raw data shows that the six intensity peaks are equal in magnitude. This is because the (111) surface of $Cd_2Re_2O_7$ contains three mirror planes and an axis of three-fold rotational symmetry. By imposing these point group symmetries on χ^S_{ijk}, the number of independent nonzero elements is greatly reduced [section S6 of (36)]. The nonlinear polarization from the surface calculated under a S_{in}–P_{out} geometry takes the simple form $\chi^S\cos(3\phi)$, where χ^S is shorthand for the χ^S_{yyy} tensor element. The resulting RA-SHG intensity pattern, which is proportional to the squared magnitude of the nonlinear polarization, exactly reproduces the high-temperature data and reaffirms its surface origin.

Upon lowering the temperature only slightly (<1 K) below T_c, we observed a dramatic change in the symmetry of the RA-SHG pattern (Fig. 3B) caused by the coherent addition of a bulk SHG contribution to the existing surface signal. Surprisingly, the data cannot be accounted for by the E_u lattice distortion alone. This is already apparent at the qualitative level because the $I\bar{4}m2$ lattice structure preserves mirror symmetry across the vertical ($1\bar{1}0$) plane (Fig. 1C), whereas the RA-SHG pattern is clearly not symmetric under a $\phi \rightarrow -\phi$ transformation. To express this analytically, the SHG susceptibility tensor in the case of E_u order contains only one independent nonzero element: $\chi^{E_u} \equiv \chi_{xyz} = \chi_{xzy} = \chi_{yxz} = \chi_{yzx} = -\chi_{zxy}/2 = -\chi_{zyx}/2$, where the Cartesian coordinates x, y, and z are chosen to be aligned along the tetragonal a, b, and c axes, respectively. With a S_{in}–P_{out} geometry, this introduces a bulk nonlinear polarization term of the form $\chi^{E_u}\cos(\phi)$ that is even in ϕ like the surface term, generating an RA-SHG pattern that is likewise even in ϕ. This is incompatible with the data and suggests that an additional inversion-symmetry–breaking order parameter emerges together with the E_u structural order parameter below T_c.

Among the four other odd-parity irreducible representations of the octahedral point group (A_{1u}, A_{2u}, T_{1u}, and T_{2u}), only an order parameter with T_{2u} symmetry can couple to the E_u structural order parameter and produce a RA-SHG pattern that breaks mirror symmetry across the ($1\bar{1}0$) plane. In the particular case of a multipolar nematic instability, it is the spin texture on the Fermi surface that explicitly breaks this mirror symmetry (Fig. 1A). The SHG susceptibility tensor associated with T_{2u} multipolar nematic
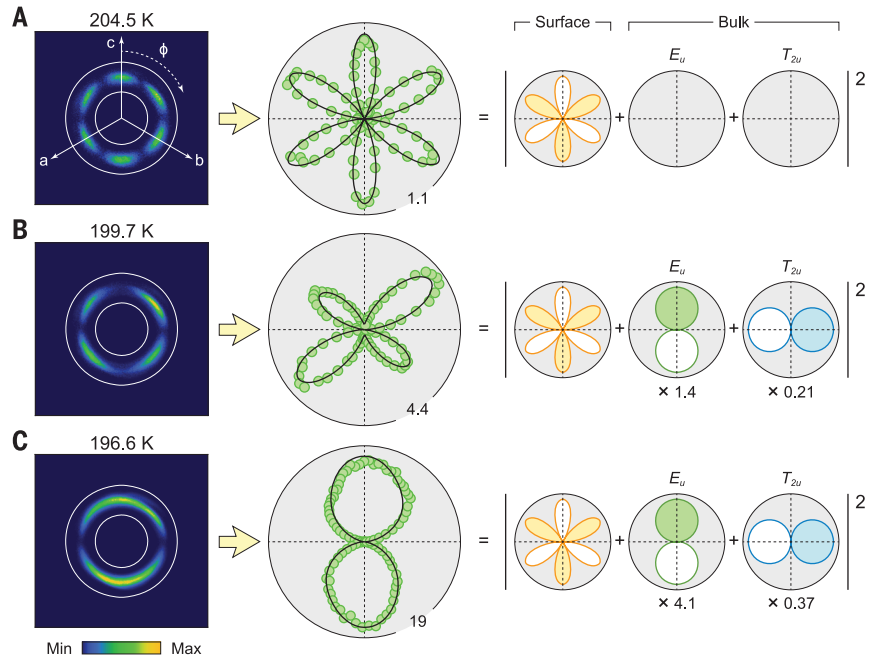

Fig. 3. Detection of E_u and T_{2u} symmetry breaking by RA-SHG. Raw RA-SHG images acquired with a S_{in}–P_{out} polarization geometry (left column) at temperatures of (**A**) 204.5 K, (**B**) 199.7 K, and (**C**) 196.6 K. Concentric white circles show the radial integration region used to generate the RA patterns (middle column). Numbers on the outer boundaries of the polar plots indicate the intensity scale in units where $\chi^S = 1$. The RA patterns are fit to the squared magnitude of a sum of surface, bulk E_u, and bulk T_{2u} polarization terms, as described in the text. Fits are overlaid on the RA patterns (black curves), and each component is illustrated in the right column, where solid petals denote a positive sign and white petals denote a negative sign for the polarization.

order ($Q_{xy} \neq 0$) contains two independent nonzero elements: $\chi^{T_{2u}} \equiv \chi_{xxz} = \chi_{xzx} = -\chi_{yyz} = -\chi_{yzy}$ and $\chi_{zxx} = -\chi_{zyy}$. The absence of any detectable bulk SHG signal in a S_{in}–S_{out} geometry [section S5 of (36)] imposes the additional constraint $\chi_{zxx} = -2\chi_{xxz}$, reducing the number of independent tensor elements to just one. For a S_{in}–P_{out} geometry, this tensor structure produces a bulk nonlinear polarization of the form $\chi^{T_{2u}}\sin(\phi)$, which taken alone would lead to a RA-SHG pattern that is even in ϕ. However, a coherent superposition of the $\chi^{T_{2u}}\sin(\phi)$, $\chi^{E_u}\cos(\phi)$, and $\chi^S\cos(3\phi)$ terms, illustrated in the right column of Fig. 3, generates a RA-SHG pattern that breaks $\phi \rightarrow -\phi$ symmetry.

To quantitatively assess the validity of this model, we performed fits to the RA-SHG data in all four polarization geometries simultaneously. We fixed χ^S at its fitted $T > T_c$ value (Fig. 3A) because it does not measurably change across T_c [section S5 of (36)], leaving the two complex numbers χ^{E_u} and $\chi^{T_{2u}}$ as the only free parameters. This model provides an excellent and unique fit to the data (Fig. 3), providing further evidence of coupled T_{2u} and E_u order parameters below T_c. As the temperature is further cooled to just several kelvin below T_c, χ^{E_u} becomes dominant, and a pronounced transformation of the RA-SHG pattern toward a $|\chi^{E_u}\cos(\phi)|^2$ form takes place (Fig. 3C), obscuring the T_{2u} order parameter. The relative faintness of the T_{2u} signal is consistent with a nematic instability that predominantly affects states only near the Fermi level and nat-

urally explains the absence of any detectable T_{2u} distortion by structure-sensitive probes (19–22).

Distinguishing a genuine electronic nematic phase transition from a simple ferrodistortive transition is a well-known experimental challenge (11) because the electronic and structural order parameters are typically coupled and have a concurrent temperature onset, as is the case for $Cd_2Re_2O_7$. The task of disentangling primary from secondary order parameters can be approached by studying the critical exponents β of the order parameter temperature scaling law $|1 - T/T_c|^\beta$. SHG is particularly well-suited for this because χ_{ijk} is linearly proportional to order parameters that are parity-odd [section S7 of (36)]. To obtain the temperature dependence of the E_u and T_{2u} order parameters, we acquired RA-SHG patterns over a series of finely spaced temperatures below T_c and fit them to the model previously described. Because $\cos(3\phi)$, $\cos(\phi)$, and $\sin(\phi)$ are orthogonal functions, the fitted values of χ^{E_u} and $\chi^{T_{2u}}$ at any given temperature can be determined uniquely. Furthermore, because the E_u and T_{2u} tensors have no elements in common, every bulk SHG response channel χ_{ijk} couples to only one of the two order parameters. The temperature dependence of $|\chi^{T_{2u}}|$, which is proportional to the T_{2u} order parameter, was extracted from such fits (Fig. 4A). An onset temperature of $T_c \approx 201$ K and a critical exponent of $\beta \approx 1/2$ are obtained from a least-squares fit to the scaling law, which is consistent
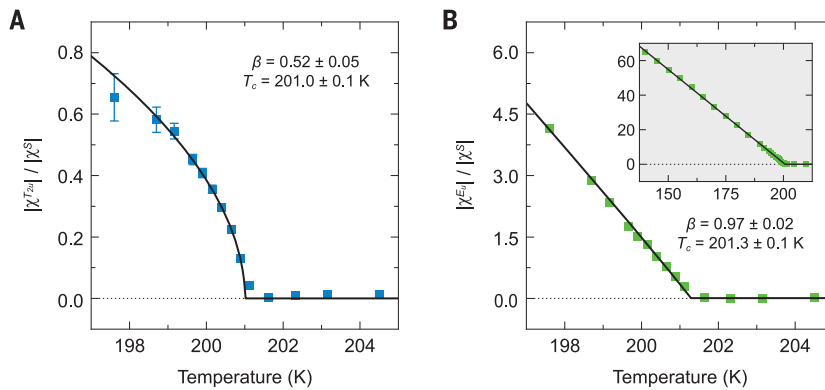
Fig. 4. Critical exponents of the T_{2u} and E_u order parameters. Temperature dependence of (**A**) $|\chi^{T_{2u}}|$ and (**B**) $|\chi^{E_u}|$ normalized to the fixed surface contribution $|\chi^S|$. Solid lines show least-squares fits to the scaling law $|1 - T/T_c|^\beta$. Specified uncertainties in the fit parameters are 1 SD. The critical exponent of the T_{2u} order parameter is consistent with the mean-field prediction $\beta = 1/2$, and the critical exponent of the E_u order parameter is consistent with a linear temperature dependence ($\beta = 1$). The inset in (B) shows that the linearity of the E_u secondary structural order persists over a wide temperature range below T_c.

with the mean-field prediction for a primary order parameter. At temperatures below ~198 K, the T_{2u} response is overwhelmed by the E_u response (Fig. 3C) and can no longer be reliably extracted from the data.

The temperature dependence of $|\chi^{E_u}|$, which is proportional to the E_u order parameter, also exhibits an onset at $T_c \approx 201$ K (Fig. 4B), demonstrating that it is coupled to the T_{2u} order parameter. It has a linear temperature dependence ($\beta \approx 1$), extending over a wide temperature range below T_c. This behavior is contrary to that expected of a primary order parameter because critical fluctuations may reduce β from its mean-field value but can never increase it. Instead, the E_u structural distortion must be a secondary order parameter. To place this interpretation on firmer theoretical grounds, we used a phenomenological Landau free-energy analysis. A system with an odd-parity primary order parameter Ψ_u and a secondary E_u order parameter Φ_{E_u} is described by the generic Landau free-energy expansion $F = F_0 - \left(1 - \frac{T}{T_c}\right)\left(a_g\Psi_g^2 + a_u\Psi_u^2\right) + b\Phi_{E_u}^2 - g\Psi_g\Psi_u\Phi_{E_u} +$ higher-order terms, where a_g, a_u, b, and g are temperature-independent parameters. To realize a linear coupling between Ψ_u and Φ_{E_u}, an additional even-parity primary order parameter Ψ_g that transforms like the product $\Psi_u\Phi_{E_u}$ must be introduced. By construction, minimization of the free energy gives $\Psi_u \propto \Psi_g \propto |1 - T/T_c|^{1/2}$ and $\Phi_{E_u} \propto \Psi_u\Psi_g \propto |1 - T/T_c|$, which exactly reproduces our experimental results. By performing a general symmetry-based analysis of the Landau expansion [section S8 of (36)], it is possible to constrain the irreducible representations of Ψ_u and Ψ_g to T_{2u} and T_{1g}, respectively. This serves as a strong self-consistency check of our RA-SHG data analysis. The T_{1g} order parameter uncovered by this analysis preserves inversion symmetry and is therefore not detectable with SHG. It is possible that interactions among elec-

trons in Re t_{2g} levels may realize a correlated spin-triplet state with T_{1g} symmetry [section S8 of (36)], and nuclear quadrupole resonance measurements have in fact detected a moderate ferromagnetic enhancement below T_c (37). Further study, however, is required to firmly establish a microscopic origin of the T_{1g} order.

Our data and analysis reveals the existence of a T_{2u} electronic order in $Cd_2Re_2O_7$ that drives the 200 K phase transition and induces the E_u lattice distortion as a secondary order parameter. The assignment of the T_{2u} order to a multipolar nematic phase is supported by previous experiments that show only weak E_u structural distortions (20–22) accompanied by large electronic anomalies across T_c (26–29), the absence of any charge or magnetic order below T_c (37), and full agreement with theoretical prediction (14). More generally, our results establish a distinct class of odd-parity multipolar electronic nematic phases in spin-orbit–coupled correlated metals and demonstrates an experimental strategy for uncovering further realizations of such order. Carefully examining the competing phases in the vicinity of odd-parity nematic order, including the superconducting phase below ~1 K in $Cd_2Re_2O_7$ (38–40), may prove fruitful for uncovering other unconventional phases of matter.

REFERENCES AND NOTES

1. E. Fradkin, S. A. Kivelson, M. J. Lawler, J. P. Eisenstein, A. P. Mackenzie, *Annu. Rev. Condens. Matter Phys.* **1**, 153–178 (2010).
2. M. P. Lilly, K. B. Cooper, J. P. Eisenstein, L. N. Pfeiffer, K. W. West, *Phys. Rev. Lett.* **82**, 394–397 (1999).
3. R. R. Du *et al.*, *Solid State Commun.* **109**, 389–394 (1999).
4. R. A. Borzi *et al.*, *Science* **315**, 214–217 (2007).
5. C. M. Varma, L. Zhu, *Phys. Rev. Lett.* **96**, 036405 (2006).
6. Y. Ando, K. Segawa, S. Komiya, A. N. Lavrov, *Phys. Rev. Lett.* **88**, 137005 (2002).
7. V. Hinkov *et al.*, *Science* **319**, 597–600 (2008).
8. T.-M. Chuang *et al.*, *Science* **327**, 181–184 (2010).
9. J.-H. Chu *et al.*, *Science* **329**, 824–826 (2010).
10. S. Kasahara *et al.*, *Nature* **486**, 382–385 (2012).
11. R. M. Fernandes, A. V. Chubukov, J. Schmalian, *Nat. Phys.* **10**, 97–104 (2014).
12. S. A. Kivelson, E. Fradkin, V. J. Emery, *Nature* **393**, 550–553 (1998).
13. C. Wu, K. Sun, E. Fradkin, S.-C. Zhang, *Phys. Rev. B* **75**, 115103 (2007).
14. L. Fu, *Phys. Rev. Lett.* **115**, 026401 (2015).
15. T. C. Lubensky, L. Radzihovsky, *Phys. Rev. E Stat. Nonlin. Soft Matter Phys.* **66**, 031704 (2002).
16. V. Kozii, L. Fu, *Phys. Rev. Lett.* **115**, 207002 (2015).
17. Y. Wang, G. Y. Cho, T. L. Hughes, E. Fradkin, *Phys. Rev. B* **93**, 134512 (2016).
18. M. R. Norman, *Phys. Rev. B* **92**, 075113 (2015).
19. C. A. Kendziora *et al.*, *Phys. Rev. Lett.* **95**, 125503 (2005).
20. J. P. Castellan *et al.*, *Phys. Rev. B* **66**, 134528 (2002).
21. J.-I. Yamaura, Z. Hiroi, *J. Phys. Soc. Jpn.* **71**, 2598–2600 (2002).
22. M. T. Weller, R. W. Hughes, J. Rooke, C. S. Knee, J. Reading, *Dalton Trans.* **2004**, 3032–3041 (2004).
23. J. C. Petersen *et al.*, *Nat. Phys.* **2**, 605–608 (2006).
24. I. A. Sergienko, S. H. Curnoe, *J. Phys. Soc. Jpn.* **72**, 1607–1610 (2003).
25. I. A. Sergienko *et al.*, *Phys. Rev. Lett.* **92**, 065501 (2004).
26. R. Jin *et al.*, *J. Phys. Condens. Matter* **14**, L117–L123 (2002).
27. N. L. Wang *et al.*, *Phys. Rev. B* **66**, 014534 (2002).
28. H. Sakai *et al.*, *Phys. Rev. B* **66**, 100509 (2002).
29. Z. Hiroi, M. Hanawa, Y. Muraoka, H. Harima, *J. Phys. Soc. Jpn.* **72**, 21–24 (2003).
30. R. W. Boyd, *Nonlinear Optics* (Academic Press, 2008).
31. L. Wu *et al.*, *Nat. Phys.* **13**, 350–355 (2017).
32. L. Zhao *et al.*, *Nat. Phys.* **12**, 32–36 (2016).
33. L. Zhao *et al.*, *Nat. Phys.* **13**, 250–254 (2017).
34. J. W. Harter, L. Niu, A. J. Woss, D. Hsieh, *Opt. Lett.* **40**, 4671–4674 (2015).
35. J. W. Harter, H. Chu, S. Jiang, N. Ni, D. Hsieh, *Phys. Rev. B* **93**, 104506 (2016).
36. Materials and methods are available as supplementary materials.
37. O. Vyaselev *et al.*, *Phys. Rev. Lett.* **89**, 017001 (2002).
38. H. Sakai *et al.*, *J. Phys. Condens. Matter* **13**, L785–L790 (2001).
39. R. Jin *et al.*, *Phys. Rev. B* **64**, 180503 (2001).
40. M. Hanawa *et al.*, *Phys. Rev. Lett.* **87**, 187001 (2001).

ACKNOWLEDGMENTS

SUPPLEMENTARY MATERIALS

Science

A parity-breaking electronic nematic phase transition in the spin-orbit coupled metal Cd$_2$Re$_2$O$_7$

J. W. Harter, Z. Y. Zhao, J.-Q. Yan, D. G. Mandrus and D. Hsieh

A nonlinear peek into electronic symmetry

Strong interactions among electrons in some materials can cause them to assume configurations that are less symmetric than the underlying crystal lattice. These so-called electronic nematic states usually have inversion symmetry, but theorists have predicted that in metals with strong spin-orbit coupling, the inversion symmetry can be lost. Harter *et al.* teased out the symmetry of the electronic order in the compound Cd$_2$Re$_2$O$_7$ (see the Perspective by Dodge). They found that a known structural transition in this material is a consequence of another, previously hidden electronic order that breaks inversion symmetry.

Science, this issue p. 295; see also p. 246

ARTICLE TOOLS	http://science.sciencemag.org/content/356/6335/295
SUPPLEMENTARY MATERIALS	http://science.sciencemag.org/content/suppl/2017/04/19/356.6335.295.DC1
RELATED CONTENT	http://science.sciencemag.org/content/sci/356/6335/246.full
REFERENCES	This article cites 51 articles, 4 of which you can access for free http://science.sciencemag.org/content/356/6335/295#BIBL
PERMISSIONS	http://www.sciencemag.org/help/reprints-and-permissions